Quantum dynamics of the $N(^4S)+O_2$ reaction on the $X\ ^2A'$ and $a\ ^4A'$ surfaces: Reaction probabilities, cross sections, rate constants, and product distributions

Paolo Defazio and Carlo Petrongolo[a)]
Dipartimento di Chimica, Università di Siena, Via A. Moro, 53100 Siena, Italy

Carolina Oliva, Miguel González, and Ramón Sayós[b)]
Departament de Química Fisica i Centre de Recerca en Química Teòrica, Universitat de Barcelona, C/Martí i Franquès 1, 08028 Barcelona, Spain

(Received 22 April 2002; accepted 29 May 2002)

We report real wave packet (WP) calculations of reaction probabilities, cross sections, rate constants, and product distributions of the reaction $N(^4S)+O_2(X\ ^3\Sigma_g^-)\rightarrow NO(X\ ^2\Pi)+O(^3P)$. We propagate initial WPs corresponding to several O_2 levels, and employ reactant coordinates and a flux method for calculating initial-state-resolved observables, or product coordinates and an asymptotic analysis for calculating state-to-state quantities. Exact or *J*-shifting calculations are carried out at total angular momentum $J=0$ or $J>0$, respectively. We employ the recent $X\ ^2A'$ S3 potential energy surface (PES) by Sayós *et al.* and the earlier $a\ ^4A'$ PES by Duff *et al.* In comparing S3 results with the WP ones of a previous $X\ ^2A'$ S2 PES, we find lower S3 energy thresholds and larger S3 probabilities, despite the higher S3 barrier. This finding is due to the different features of the doublet PESs in the reactant and product channels, at the transition state, and in the NO_2 equilibrium region. We analyze the effects of the O_2 initial level and show that tunneling through the S3 barrier enhance the room-temperature rate constant by ~3.7 times with respect to the previous S2 WP rate. The agreement with the room-temperature experimental result is thus notably improved. The NO vibrational distribution is inverted and the rotational ones are strongly oscillating. We explain these nonstatistical results showing that the reaction partners approach each other with a large impact parameter. The WP vibrational distribution is however different from that observed, which is oscillating. WP calculations show that the new S3 PES describes accurately several features of the $X\ ^2A'$ state, although a lowering of its barrier height by ~0.56 kcal/mol should bring calculated and observed rate constants in full agreement. © *2002 American Institute of Physics.*
[DOI: 10.1063/1.1494781]

I. INTRODUCTION

The reaction $N(^4S)+O_2(X\ ^3\Sigma_g^-)\rightarrow NO(X\ ^2\Pi)+O(^3P)$ is involved in important atmospheric and combustion processes, and has been therefore the subject of many investigations. It is exoergic by 1.38 eV and NO products are thus formed with high vibrational and rotational quanta. The thermal rate constant has been measured between 298 and 5000 K, and the activation energy is equal to 0.28 eV.[1] Product vibrational distributions have been measured at room temperature[2] or at collision energy of about 3 eV.[3] The reactants and products correlate adiabatically to the lowest doublet $X\ ^2A'$ and quartet $a\ ^4A'$ electronic states of NOO in C_s symmetry, neglecting spin–orbit couplings.

The first theoretical work on this reaction dates back to 1987, when Walch and Jaffe[4] calculated C_s *ab initio* potential energy surfaces (PES) of $X\ ^2A'$ and $a\ ^4A'$. Later on, analytical PESs, reaction probabilities, cross sections, rate constants, and product distributions have been calculated employing different methods. Recently, we have begun an extensive theoretical study of the $X\ ^2A'$ and $a\ ^4A'$ surfaces, and of kinetic and dynamical properties of this reaction. We have thus obtained new *ab initio* PESs for describing C_s abstraction and insertion mechanisms.[5] Insertions and conical intersections in C_{2v} symmetry were also investigated.[6] We have then calculated analytical fits to both surfaces and vibrational-transition-state-theory (VTST) rate constants.[7] Finally, we have carried out the first quantum-mechanical study of the reaction dynamics,[8] employing an earlier doublet PES (Ref. 9, labeled here S2) and a time-dependent wave packet (WP) approach. The height of the reaction barrier is 0.27 eV for the S2 surface of Ref. 9 or 0.30 eV for our new surface described in Ref. 7 (labeled here S3). However, the S3 PES improves considerably the description of the NO_2 ground electronic state, because the $X\ ^2A'$ well depth and geometry are in good agreement with experimental data, contrary to S2 results. This feature is important in quasiclassical trajectory (QCT) calculations, since trajectories can enter into the NO_2 minimum region.[7,10] Moreover, a correct description of this region is even more important in WP calculations that depend on all details of the PESs, as we stressed in Ref. 8 and we shall show in the present work. Thus, a new WP investigation of the reaction dynamics on

a)Electronic mail: petrongolo@cuces.unisi.it
b)Electronic mail: r.sayos@qf.ub.es

TABLE I. Stationary point properties of the $X\ ^2A'$ and $a\ ^4A'$ potential surfaces of NO_2. Energies in eV, distances in a_0, angles in deg, and frequencies in cm^{-1}.[a]

		$X\ ^2A'$	$a\ ^4A'$
$N+O_2$	Energy	0.0	0.0
	R(OO)	2.28	2.28
NO+O	Energy	−1.41	−1.41
	R(NO)	2.19	2.19
Barrier	Energy	0.30	0.65
	R(NO)	3.59	3.43
	R(OO)	2.33	2.33
	<(NOO)	109	107
	Frequencies[b]	1221, 399, *486i* (1605, 382, 303*i*)[c]	1416, 394, *307i*
NO_2 C_{2v} minimum	Energy	−4.71	−7.94
	R(NO)	2.30	2.19
	<(ONO)	126	180

[a]$X\ ^2A'$ S3 surface from Ref. 7 and $a\ ^4A'$ surface from Ref. 11.
[b]The first two values refer to the OO stretching and to the NOO bending, respectively.
[c]S2 values of Ref. 9.

both doublet and quartet PESs is highly advisable, and we report here the results of such a study, employing the recent $X\ ^2A'$ S3 surface by Sayós *et al.*[7] and the previous $a\ ^4A'$ analytical PES by Duff *et al.*,[11] whose barrier height is equal to 0.65 eV. Table I shows stationary point properties of the surfaces here employed.

Although we have recently calculated a new analytical quartet surface,[7] based on 910 *ab initio* points,[5] this PES has an artificial $D_{\infty h}$ barrier along the O+N+O product channel, at an OO distance of about 7.6 bohr and at about 23 eV above the $N+O_2$ asymptote. This $D_{\infty h}$ barrier does not affect VTST calculations,[7] which depend mainly on the PES shape near the reaction barrier, or QCT results,[10] because very few trajectories sample this highly repulsive region of the surface. On the contrary, WP calculations of reaction probabilities are very sensitive to all features of the surface. Therefore, this artificial $D_{\infty h}$ barrier has a deep impact on WP results, reflecting back part of the WP and giving unphysical reaction probabilities at collision energies $\gtrsim$1.2 eV. In future work, we shall calculate more *ab initio* points and we shall fit better this repulsive region of the quartet PES.

We describe the theoretical method in Sec. II. Section III presents reaction probabilities and dynamics at total angular momentum quantum number $J=0$. Section IV reports J-shifting cross sections and rate constants, and we discuss in Sec. V vibrorotational NO product distributions. We finally present our conclusions in Sec. VI.

II. METHODS

Gray and Balint-Kurti[12] (GBK) have recently developed an accurate and efficient time-dependent formalism for investigating the quantum dynamics in triatomic systems, merging the advantages of some previous approaches. Consider a reactive collision $A+BC(v,j)\rightarrow AB(v',j')+C$ and define an initial WP, associated with an electronic state of ABC and with a vibrorotational level (v,j) of BC. The equation of motion is solved via a $\cos^{-1}$ mapping of a scaled Hamiltonian, with eigenvalues in $(-1,1)$, resulting in a simple Chebyshev recursion. Only the real part of the WP is propagated, and the computational effort is thus reduced two times with respect to the propagation of a complex WP. Grid or Legendre representations of radial or angular nuclear coordinates are implemented via fast Fourier transforms or discrete variable representations, respectively. State-to-state reaction probabilities $P^J_{v'j',vj}(E_{\rm col})$, at J and collision energies $E_{\rm col}$, are then obtained propagating the WP in product coordinates and performing an asymptotic analysis.[12] On the other hand, initial-state-resolved reaction probabilities $P^J_{vj}(E_{\rm col})$ are calculated propagating the WP in reactant coordinates and performing a flux analysis.[13] The GBK method has been extended to nonadiabatic reactions[14] and to exact calculations at $J>0$.[15]

We have employed the GBK approach for calculating exact reaction probabilities at $J=0$, and we have estimated the probabilities at $J>0$ via the J-shifting (JS) approximation,[16] as implemented in Refs. 8 and 17 for bent transition states. We have used the following rotational constants of the transition states (TS): $\bar{B}^{\neq}=0.31$ and $(\bar{A}^{\neq}-\bar{B}^{\neq})=1.94\ \mathrm{cm}^{-1}$ for $X\ ^2A'$, $\bar{B}^{\neq}=0.34$ and $(\bar{A}^{\neq}-\bar{B}^{\neq})=1.86\ \mathrm{cm}^{-1}$ for $a\ ^4A'$. Cross sections $\sigma_{v'j',vj}(E_{\rm col})$ and $\sigma_{vj}(E_{\rm col})$ and rate constants $k_{v'j',vj}(T)$, $k_{vj}(T)$, and $k(T)$ at temperature T have been obtained through the usual expressions, including the electronic degeneracies 1/6 or 1/3 for $X\ ^2A'$ or $a\ ^4A'$ rates, respectively.

Taking into account the Pauli principle for $O_2(X\ ^3\Sigma_g^-)$,[18] we consider only odd j values up to $j=11$. Initial-state-resolved observables and thermal rate constants have been calculated for $v=0$ and 1, employing both $X\ ^2A'$ and $a\ ^4A'$ PESs and $N+O_2$ Jacobi coordinates R, r, and γ. State-to-state quantities of NO vibrorotational distributions at $T=300$ K have been obtained for $v=0$, using the $X\ ^2A'$ PES and NO+O Jacobi coordinates R', r', and γ', and transforming the initial WP from the reactant to the product channel. Other details of the method are described in Refs. 8, 12, and 13, and Table II reports the parameters of the calculations for both reactant and product runs. The dimension of the reactant or product representation are equal to 3 240 650 or 2 429 520, respectively.

TABLE II. Parameters of the calculations.[a]

	Reactant run	Product run
Translational energy center of the initial WP	0.6 ($X\ ^2A'$) and 0.9 eV ($a\ ^4A'$)	0.6 ($X\ ^2A'$)
R center and width of the initial WP	10 and 0.1	10 and 0.2
R range and No. of grid points	0–14.5 and 329	0–12 and 191
r range and No. of grid points	1.5–11.5 and 197	1.5–11.5 and 159
No. of Legendre polynomials and of γ points	50 ($j''=1,3,\ldots,99$)	80 ($j''=0,1,\ldots,79$)
Potential and centrifugal cutoff	0.44	0.44
R and r absorption start at	11.5 and 8.5	9 and 8.5
R and r absorption strength	0.01	0.01
Flux analysis at r	7	
Asymptotic analysis at R		8.5

[a]Values in a.u. unless otherwise specified.

III. $J=0$ REACTION PROBABILITIES AND DYNAMICS

Because the $N+O_2$ reaction is exoergic, with a barrier in the entrance channel, static or dynamical effects should dominate the mechanism at low or high E_{col}, respectively. The analysis of the reaction probabilities at $J=0$ gives detailed information on the dynamics, which confirm this expectation. Since the reactant-run representation of Table II and that of Ref. 8 give very similar probabilities up to $E_{col} \approx 0.7$ eV, we can contrast the present S3 results with the earlier S2 ones at low E_{col}. The effects of the potential are more remarkable in this low-energy regime, whereas at higher energies the results depend more on the O_2 initial state and on the energy distribution between the translational and internal degrees of freedom.

As an example, Fig. 1(a) shows $P^0_{0,9}$ of $O_2(0,9)$, the most populated level at room T, for both doublet surfaces. The S3 probabilities are larger than the S2 ones up to about 0.35 eV and the reaction has thus lower energy thresholds on the S3 PES, whereas the S2 surface is more reactive between 0.4 and 0.7 eV. Since the S3 barrier height is 0.03 eV greater than the S2 one, the enhancement of the reactivity near the threshold is a somewhat surprising result, which shows that the detailed dynamics depends on other features of the PESs that compensate the effect of the barrier height.

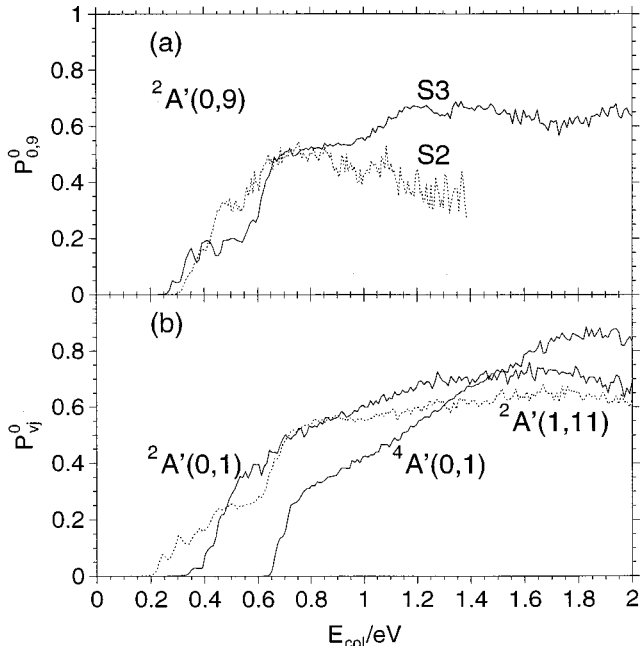

FIG. 1. (a) Reaction probabilities $P^0_{0,9}$ for S3 (full line) and S2 (dotted line) PESs. (b) Reaction probabilities for S3 $^2A'(0,1)$ (full line) and $^2A'(1,11)$ (dotted line), and for $^4A'(0,1)$ (full line).

First note that the S3 O_2 and NO vibrorotational energies are respectively higher and smaller than the S2 energies. This implies that the reactant channel is narrower and steeper on the S3 PES than on the S2 surface, whereas the opposite is true for the product arrangement. At low E_{col}, the S3 wave packet is thus more localized along the entrance minimum energy path (MEP) and more flux can enter into the exit channel. Both these behaviors increase the reactivity in the low energy regime.

The shape of the surfaces near their TSs is a second compensating effect. Table I shows indeed that the OO stretching frequency is smaller on S3, implying that the OO bond breaks more easily on this surface, thus increasing the S3 reactivity at low E_{col}. Moreover the larger S3 imaginary frequency hints at a narrower barrier, and thus at a faster breaking rate of the TS and at a larger tunnel effect. By comparing indeed the static thresholds with the dynamical ones, we find an S3 tunneling at $v=0$ and for any j value, whereas the S2 tunneling occurs only at $(v,j)=(0,11)$.

Finally, we have already shown[8] that the NO_2 minimum region of the doublet PES can trap part of the wave packet. The intermediate complexes will give either the reactants or the products, thus lowering the reactivity with respect to a direct collision. Because the NO_2 well depth is equal to 7.96 or 4.71 eV in the S2 or S3 PES, respectively, this capture mechanism is less important for the S3 surface that is then more reactive.

These different features of the doublet PESs in the reactant and product channels, at the TS, and in the minimum region thus increase the S3 reaction probabilities at low E_{col} and have a deep impact on the rate constant at low temperature, as we shall see in Sec. IV.

Figure 1(b) shows the $O_2(v,j)$ effects on the S3 dynamics, by comparing the reaction probabilities associated with the O_2 ground state (0,1) and with the most excited state (1,11) here considered. The O_2 initial excitation enhances the

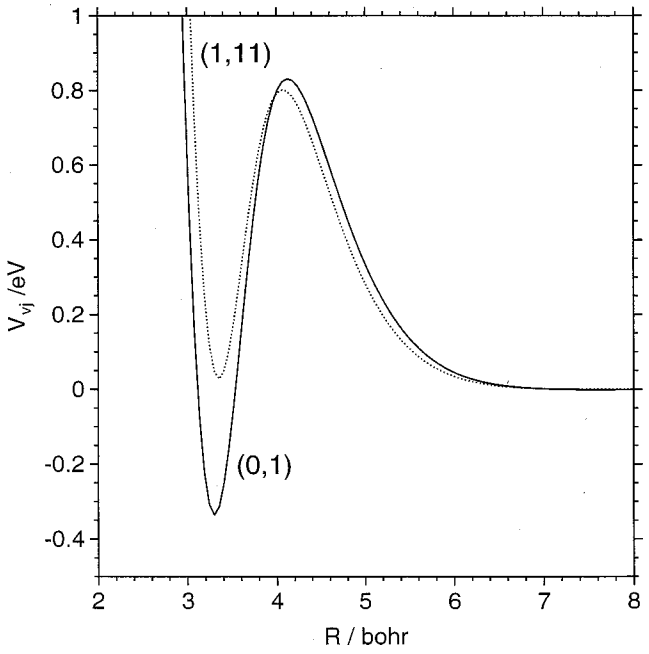

FIG. 2. Effective potentials $V_{0,1}$ (full line) and $V_{1,11}$ (dotted line).

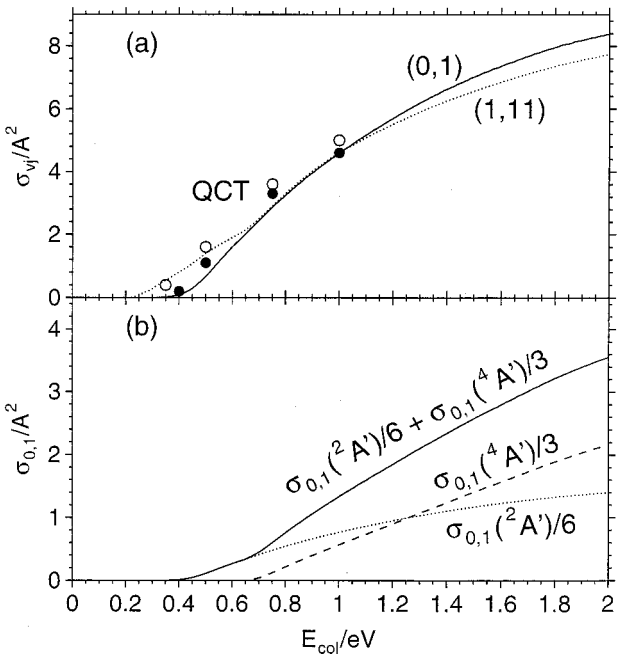

FIG. 3. (a) $X\ ^2A'$ WP and QCT cross sections $\sigma_{0,1}$ (full line and filled circles, respectively) and $\sigma_{1,11}$ (dotted line and empty circles, respectively). (b) Cross section $\sigma_{0,1}$ for $X\ ^2A'$ (dotted line), $a\ ^4A'$ (dotted line), and their sum (full line), including the electronic degeneracies.

probability near the threshold, but slightly inhibits the reactivity at high energy. These (v,j) effects at low E_{col} can be understood looking at the effective potentials,

$$V_{vj}(R)=\langle \phi_{vj}^{O_2}(r)\overline{P}_j(\gamma)|V(R,r,\gamma) - V^{O_2}(r)|\phi_{vj}^{O_2}(r)\overline{P}_j(\gamma)\rangle_{r\gamma}+j(j+1)/2\mu_R R^2, \tag{1}$$

which influence the initial wave-packet dynamics.[19] In Eq. (1), $\phi_{vj}^{O_2}$ is the O_2 initial state, $\overline{P}_j$ is a normalized Legendre polynomial, V is the doublet S3 PES, V^{O_2} is the O_2 potential, and μ_R is the reduced mass associated with R. Figure 2 shows that $V_{0,1}$ and $V_{1,11}$ have a barrier at $R=4$ bohr and a minimum at $R\approx 3.3$ bohr, and that the $V_{1,11}$ barrier is lower than the $V_{0,1}$ one. This finding thus explains why the low-energy reaction probabilities increase with the O_2 quanta, and implies that (v,j) effects reflect the shape of $V_{vj}(R)$.

Figure 1(b) reports also an example of a reaction probability on the $a\ ^4A'$ surface. The quartet threshold is about 0.35 eV greater than the doublet threshold, as expected from the different barrier heights. The $^4A'$ probabilities rise steeper with E_{col} than the $^2A'$ ones, and the quartet reactivity is thus larger than the doublet one above 1.4 eV.

IV. CROSS SECTIONS AND RATE CONSTANTS

The results of this section have been obtained using the S3 $X\ ^2A'$ surface[7] and the $a\ ^2A'$ surface of Ref. 11. When O_2 is in the ground level (0,1), the collision energy threshold attains the highest value, equal to 0.19 eV. The threshold is reduced at high O_2 quanta, up to the minimum value of 0.05 eV for $(v,j)=(1,11)$, which is the highest O_2 level here considered. We have estimated the reaction threshold at various temperatures, averaging the initial-state-resolved thresholds over a Boltzmann distribution of the O_2 initial levels. This average threshold is equal to 0.16 eV at 300 K, close to the value of 0.15 eV for the most populated $O_2(0,9)$ level at this temperature, and it is reduced to 0.13 eV at 3000 K.

Figure 3(a) shows the doublet WP and QCT cross sections for O_2 initial levels $(v,j)=(0,1)$ and (1,11). The trend of $\sigma_{vj}(E_{\mathrm{col}})$ with respect to E_{col}, v, and j is similar to that of the probabilities. High O_2 vibrorotational quanta thus enhance or lower S3 $\sigma_{vj}(E_{\mathrm{col}})$ at low or high E_{col}, respectively. QCT and WP cross sections on the new doublet PES are in close agreement, and also agree quite well with previous semiclassical results on other surfaces.[20,21] Figure 3(b) presents the cross sections for $O_2(0,1)$, considering the electronic degeneracy factors 1/6 and 1/3 for $X\ ^2A'$ and $a\ ^4A'$, respectively. We see that the doublet $\sigma_{0,1}$ is larger than the quartet one up to $E_{\mathrm{col}}\approx 1.2$ eV, whereas the opposite holds at higher energies in agreement with the probability results of the previous section and with QCT calculations.[10]

The variation of the degeneracy-averaged cross sections vs the O_2 initial excitation is reported in Fig. 4 at two collision energies: 0.5 eV, where only the $X\ ^2A'$ channel is open, and 1.5 eV, where the $a\ ^4A'$ channel dominates. The trend of the cross sections with respect to v and j confirms that of the reaction probabilities, and shows that σ_{vj} oscillate with j and increase with v. At both collision energies, one O_2 vibrational quantum enhances the cross sections, whereas the most reactive O_2 rotational level depends on the collision energy. Figure 4 shows indeed that $\sigma_{1,j}$ is maximum at $j=11$ or 5 at $E_{\mathrm{col}}=0.5$ or 1.5 eV, respectively.

We have calculated initial-state-resolved rate constants $k_{vj}(T)$ for both doublet and quartet PESs as Boltzmann averages over the collision energy and the cross section, includ-

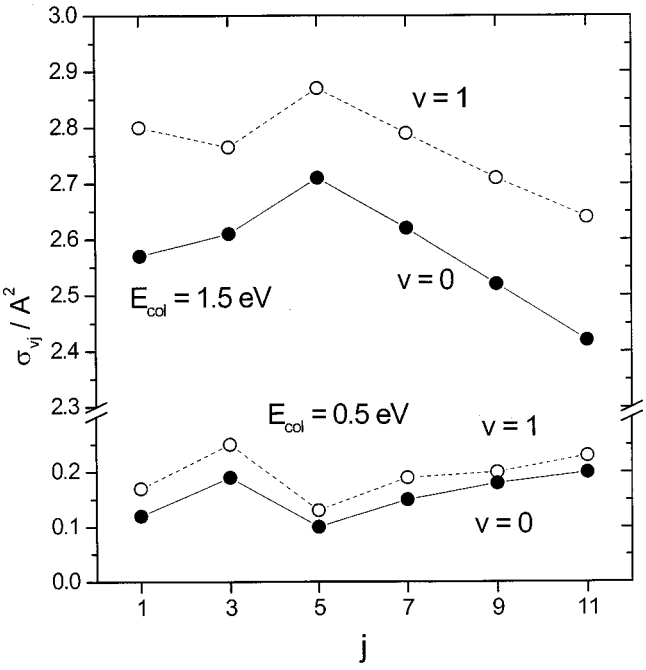

FIG. 4. Degeneracy-averaged cross sections at $E_{col}=0.5$ and 1.5 eV, and at $v=0$ (full line) and 1 (dotted line).

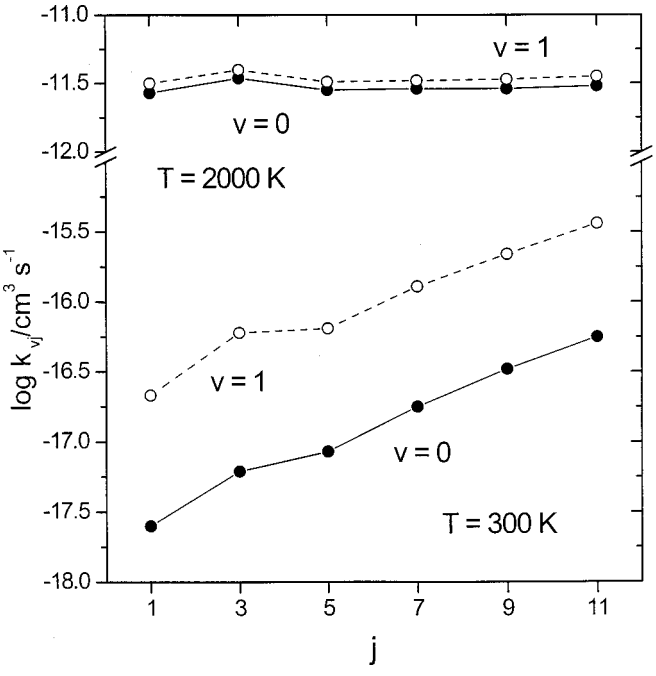

FIG. 5. Initial-state-resolved rate constants at 300 and 2000 K, and at $\nu=0$ (full line) and 1 (dotted line).

ing the electronic degeneracies,[22(a)] and we show in Fig. 5 these rates at $T=300$ and 2000 K. At room temperature, $k_{vj}(T)$ increase nearly exponentially with j, and are enhanced more than two orders of magnitude increasing (v,j) from (0,1) to (1,11). The O_2 rotational excitation is about three times more effective than the vibrational one in increasing k_{vj}. Of course, these (v,j) effects are strongly reduced at 2000 K, where the rates are scarcely influenced by the O_2 initial level.

Thermal rate constants $k(T)$ have been obtained as Boltzmann averages over the $k_{vj}(T)$ rates. To this end, we have explicit calculated k_{vj} ($v=2$ and 3, $j=11$) for both electronic states, we have estimated k_{vj} ($v=2$ and 3, $j<11$) with linear extrapolations as $k_{1,j}(k_{v,11}/k_{1,11})$, and we have assumed that k_{vj} $(j>11)\approx k_{v,11}$. Figure 5 shows that this procedure should underestimate the room-T rate constant, because k_{vj} increases with j, but that it should be correct at high T where k_{vj} do not vary with j.

Table III and Fig. 6 show that the WP thermal rate constants are about two times smaller than the experimental ones[1] at low T, whereas the WP results are within the experimental error bars at $T>1000$ K. This finding can be due to an overestimation of the barrier heights of both PESs. However, the *ab initio*[5] value of the $X\ ^2A'$ S3 barrier height has been increased by 0.09 eV in the analytical PES,[7] for obtaining the best agreement between VTST and experimental data at 300 K. This VTST barrier scaling seems too large for the WP $k(T)$, because a numerical experiment has shown that a lowering of the σ_{vj} thresholds by only 0.0245 eV yields WP and observed rates is nearly full agreement.

TABLE III. Temperature in K and rate constants in cm^3 s^{-1}.

T	This work	Experiment[a]	
		k	Error limits(Δ log k)
300	3.53×10^{-17}	8.31×10^{-17}	±0.12
600	1.55×10^{-14}	3.87×10^{-14}	±0.12
1000	2.39×10^{-13}	5.70 ± 10^{-13}	±0.12
1500	1.22×10^{-12}	2.54×10^{-12}	±0.3
2000	3.23×10^{-12}	5.85×10^{-12}	±0.3
3000	9.88×10^{-12}	1.51×10^{-11}	±0.3

[a]Reference 1.

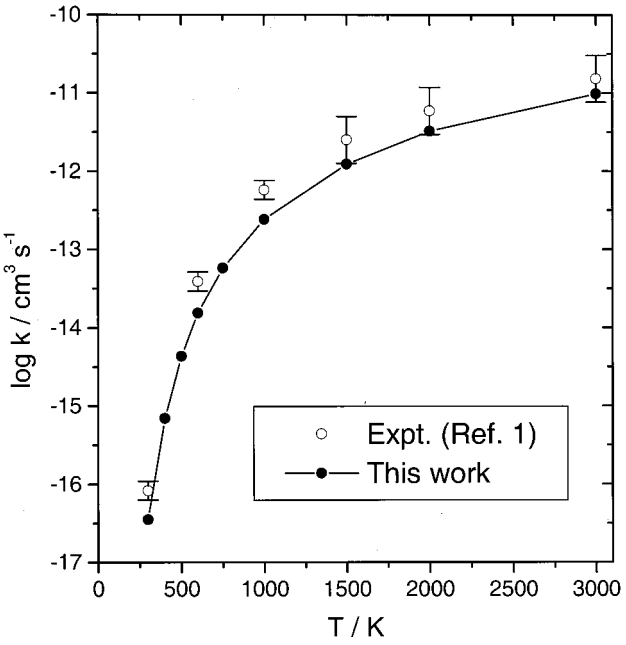

FIG. 6. Calculated (full line) and observed (empty circles, with error bars) thermal rate constants.

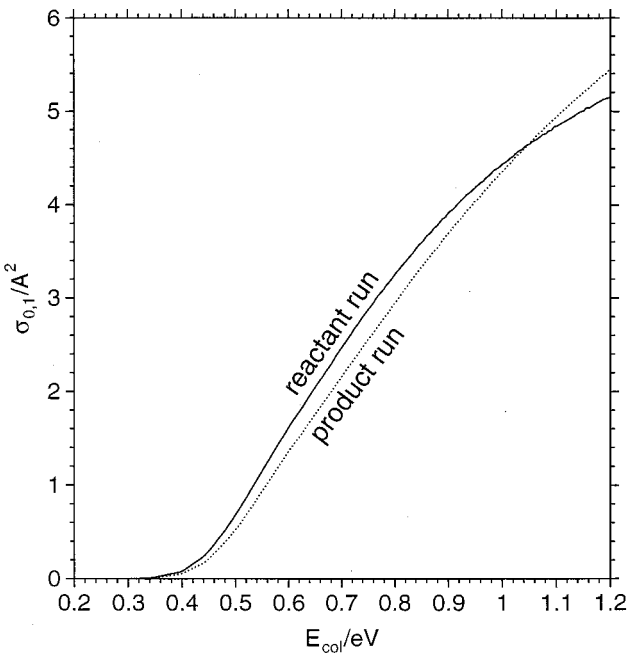

FIG. 7. S3 cross section $\sigma_{0,1}$, calculated with the reactant (full line) or product run (dotted line).

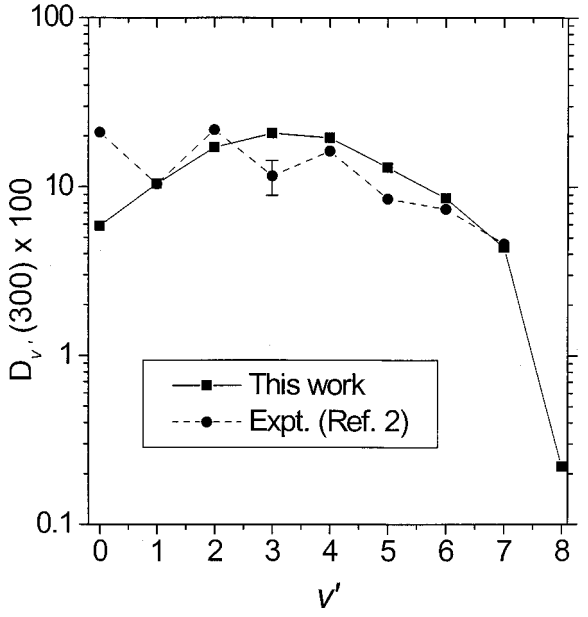

FIG. 8. Vibrational product distribution of NO(v') for reactants at 300 K. S3 calculated (full line) and experimental (dashed line) results.

We have seen in Sec. III that the energy thresholds are smaller and the reaction probabilities at low E_{col} are larger on the present $X\ ^2A'$ S3 PES than on the earlier S2 surface.[8] Therefore, the S3 thermal rate constants at low T are considerably larger than the S2 ones, thus improving the agreement between WP and observed rates. S3 (S2) $k(300)$ and $k(600)$ are indeed equal to 3.52×10^{-17} (9.5×10^{-18}) and 1.54×10^{-14} (8.9×10^{-15}) cm^3 s^{-1}, respectively, i.e., the S3 k are larger than the S2 ones by $\sim$3.7 or 1.7 times at 300 or 600 K, respectively. As we have discussed in Sec. III, these S3 results are due to the PES shape in the reactant and product channels, to the TS vibrational frequencies, to a large tunneling through the barrier, and to a smaller NO_2 minimum. Moreover, the smaller OO stretching frequency of the S3 TS, with respect to the S2 one, implies that the number of available states at the TS is larger in the S3 surface. In statistical terms, this corresponds to a larger S3 partition function and therefore to a larger k.

At $T<1000$ K, S3 VTST rate constants[7] are lower than the S2 ones, in agreement with the higher S3 barrier but contrary to the present WP results. Because statistical results do not take into account quantum effects and depend mainly on the barrier region of the PES, this comparison highlights important quantum effects near the S3 reaction threshold and the role of the overall surface.

V. PRODUCT DISTRIBUTIONS

In this section we present vibrorotational distributions of NO(v',j') products, at $E_{col}\leqslant1.2$ eV and at room temperature. These calculations were carried out by propagating wave packets in product coordinates, and employing the $X\ ^2A'$ S3 PES, six O_2 levels with $v=0$ and $j\leqslant11$, and the product-run representation of Table II. Initial-state-resolved probabilities, cross sections and rate constants are very similar in both propagations, as Fig. 7 shows for $\sigma_{0,1}$. The rate constant $k_{0,1}(300)$ is equal to 3.53×10^{-18} or 3.42×10^{-18} cm^3 s^{-1}, and the thermal rate $k(300)$ is equal to 3.50×10^{-17} or 3.81×10^{-17} cm^3 s^{-1} in the reactant or product run, respectively. This level of agreement is actually pretty good, considering that very different coordinates and dimensions are used in the two runs.

We have compared the calculated and experimental[2] vibrational distributions of NO(v') at 300 K. Recently, Caledonia *et al.*[3] measured a vibrational distribution at $E_{col}\approx3$ eV. The WP calculation of this distribution at 3 eV would require product propagations on both doublet and quartet PESs and $v=0$ and 1, doubling the reactant run representation of Table II, and this is beyond our present computer capabilities.

Figure 8 shows the vibrational distribution of NO(v') for reactants at $T=300$ K,

$$D_{v'}(T)=k_{v'}(T)\Big/\sum_{v'}k_{v'}(T), \tag{2}$$

where $k_{v'}(T)$ are the rate constants for the production of NO(v'). These rates have been calculated from the state-to-state $k_{v'j',0j}(T)$ for $N+O_2(0,j)\rightarrow NO(v',j')+O$, averaging over a Boltzmann distribution at T of the j levels and summing over the j' levels. The quantum-mechanical distribution is inverted, peaking at $v'_{max}=3$, and is qualitatively similar to the semi-classical distributions that are also inverted, with $v'_{max}=1$,[10] 2,[23] or 4,[11] according to the theoretical treatment employed. Increasing the temperature, the population shifts to higher v' values, as expected, and the maximum at 1000 K is at $v'_{max}=4$. Note that the calculated vibrational distribution is different from the prior vibrational distribution, which assumes that all product states are equally probable.[22(b)]

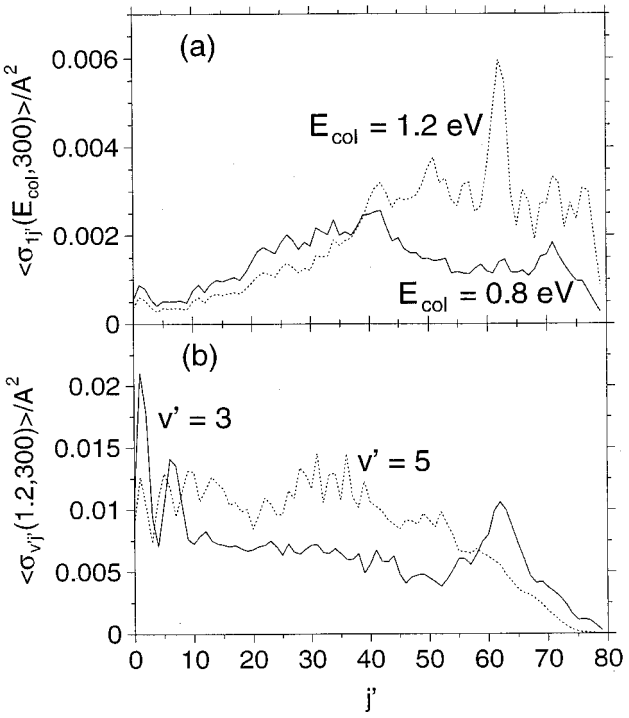

FIG. 9. S3 rotational product distributions of NO(v',j') for reactants at 300 K. (a) $E_{col}=0.8$ (full line) or 1.2 (dotted line) eV, and $v'=1$. (b) $E_{col}=1.2$ eV, and $v'=3$ (full line) or 5 (dotted line).

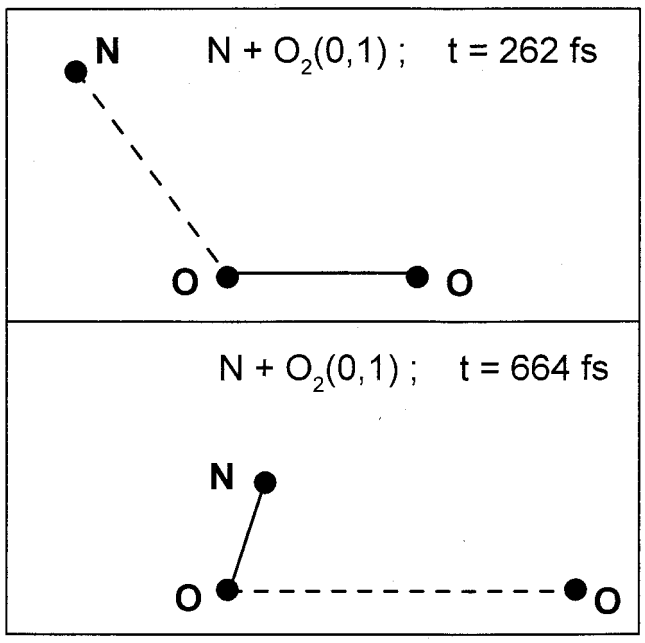

FIG. 10. N+O_2(0,1) and S3 PES. Nuclear snapshots at $t=262$ and 664 fs. Full or dashed lines show actual or broken bonds, respectively.

We report in Fig. 9 the rotational distributions $\langle\sigma_{v'j'}(E_{col},T)\rangle$ of NO for reactants at $T=300$ K, for $v'=1$ in panel (a), and for $v'=3$ and 5 in panel (b), where the cross-section scales are different in the two panels. The collision energies are equal to 0.8 and 1.2 eV above and to 1.2 eV below. These results have been obtained from state-to-state cross sections $\sigma_{v'j',0j}(E_{col})$, averaging over a Boltzmann distribution of the $O_2(0,j)$ levels. Even more than the vibrational distribution, the rotational populations depend on dynamical effects, as the opening and closing of many NO(v',j') channels and the energy redistribution among the product degrees of freedom. The rotational distributions are indeed strongly oscillating, different from the prior rotational distributions,[22(b)] and high NO rotational quanta are in general preferred. At large E_{col}, the collision is highly selective with respect to j', because only a few NO rotational levels are preferentially populated. This last finding confirms that the high-energy dynamics is predominantly direct. The distribution at $v'=1$ and $E_{col}=0.8$ is maximum at $j'_{max}=42$ and 71, and the distribution at $E_{col}=1.2$ eV is strongly peaked at $j'=62$. Increasing v' from 1 to 3, the distribution at $E_{col}=1.2$ is still oscillating, but the favored j' levels are now equal to 1 (strongly preferred), 6, and 62. Figures 8 and 9(a) show that the N+O_2 collision at room T and $E_{col}=1.2$ eV gives preferentially NO products with $v'=3$ and $j'=1$. However, the rotational distributions depend strongly on v', as Fig. 9 shows for $E_{col}=1.2$ eV and $v'=1$, 3, and 5.

The calculated product distributions are consistent with the usual rules of an exoergic abstraction reaction, which is dynamically controlled and whose barrier is in the entrance channel.[22(c)] The inverted vibrational population of NO(v') is also consistent with the stretched NO bond of the TS.[7] These results can be explained looking at the expectation values of the reactant radial coordinates $\langle R(t)\rangle$ and $\langle r(t)\rangle$ and at the reactant average angle $\overline{\gamma}(t)$ at time t (see Ref. 8 for more details). For N+O_2(0,1) and the S3 PES, Fig. 10 reports two nuclear snapshots at $t\approx262$ and 664 fs, and shows that the N atom approaches O_2 with a large impact parameter b, forming the NO bond with the first O atom whereas the second oxygen goes away. This large b favors high v' and j' quanta of the NO products, whose vibrational distribution is thus inverted and the rotational one is oscillating with high j' levels populated at any v'. From the comparison with the prior statistical distributions, we conclude that the detailed reaction dynamics is highly not statistical.

Figure 8 shows that the calculated WP vibrational distribution of NO(v') is in satisfactory agreement with that observed[2] at room T, for $v'=1$, 2, and $\geqslant4$. Our population at 300 K compares also rather well with that measured at $E_{col}\approx3$ eV,[3] except at $v'=3$. Both experimental distributions are however oscillating and even v' levels are preferred, in contrast to all the theoretical results. Observed and calculated populations are mainly different at $v'=0$ and 3, but we have not been able to reproduce the experiments, despite many long calculations. Probably, the $X\,^2A'$ S3 PES and the J-shifting approximation are not accurate enough to obtain a subtle quantity as the product distribution in this reaction that involves three heavy nuclei. However, Winkler *et al.*[2] have shown that the NO vibrational quenching in NO+O_2 is at least 150 times faster than the NO formation in N+O_2, implying that this quenching can bias the results at room T of Ref. 2. This effect should indeed give a $v'=0$ experimental population much larger than that calculated. On the other hand, Caledonia *et al.*[3] rule out the NO quenching at 3 eV, and therefore further theoretical and experimental works seem necessary for checking the NO(v') distribution.

VI. CONCLUSIONS

This paper reports a wave packet study of several dynamical and kinetic properties of the reaction $N(^4S) + O_2(X\ ^3\Sigma_g^-) \rightarrow NO(X\ ^2\Pi) + O(^3P)$ on the $X\ ^2A'$ and $a\ ^4A'$ PESs. We have employed the real wave packet formalism by Gray and Balint-Kurti,[12] who obtain the scattering S matrix and total probabilities solving a modified time dependent Schrödinger equation and performing asymptotic[12] or flux analyses.[13] We have propagated up to twelve initial wave packets corresponding to $O_2(v,j)$ vibrorotational levels with $v \leqslant 1$ and $j \leqslant 11$. We have employed reactant propagations and the flux method for calculating initial-state-resolved reaction probabilities, cross sections, and rate constants. State-to-state dynamical observables and product vibrorotational distributions have been obtained through product propagations and the asymptotic analysis. Large grid and Legendre representations have been used, up to 3 240 650 dimensions. We have calculated exact or J-shifting probabilities at $J=0$ or $J>0$, respectively, and we have discussed some elementary dynamical processes by analyzing probabilities and product distributions.

We have employed the recent S3 doublet PES by Sayós *et al.*,[7] which agrees well with all the experimental information on the stationary points of the NO_2 ground surface. This PES thus improves notably the previous surfaces of Refs. 9 and 11, which do not describe correctly the $NO_2\ X\ ^2A_1$ equilibrium region. The correct S3 shape is very important in WP calculations that are sensitive to all the features of the surface. On the other hand, we have employed the earlier quartet PES by Duff *et al.*,[11] because an artificial barrier of the new quartet PES of Ref. 7 prevents us from using the WP approach, although this repulsive region of the PES was not important in VTST (Ref. 7) or QCT (Ref. 10) studies.

The collision proceeds on the S3 surface with a lower energy threshold with respect to the S2 threshold, so that the S3 surface is more reactive despite its higher barrier. We have ascribed this result to three features of the S3 PES. (i) The shape of the reactant and product channels, which increases the localization of the WP along the entrance MEP and the flux through the exit surface. (ii) The frequency values and the narrower barrier of the S3 TS, which favor the breaking of the O_2 diatom and of the TS, and increase tunnel effects. (iii) The lower S3 hole of the NO_2 bound geometry that captures less WP with respect to that of the S2 surface, thus increasing the reactivity.

We have discussed the effects of the O_2 initial excitation in terms of the effective potential felt by the WP along its motion from the reactant channel into the interaction region. The WP cross sections are close to the QCT (Ref. 10) ones; they are enhanced by one O_2 vibrational quantum and oscillate somewhat with j. The present study improves considerably the agreement between calculated and observed rate constants at low temperatures, with respect to previous WP calculations.[8] Moreover, the accord becomes nearly quantitative provided the S3 analytical barrier height is lowered by 0.0245 eV. WP calculations also show that S3 quantum tunnel effects are very important at room temperature and are remarkable up to about 600 K.

The WP vibrational distribution of the $NO(v')$ products is inverted at 300 K, and NO is preferentially formed with $v'=3$. The product rotational populations are strongly oscillating. These nonstatistical results agree qualitatively with previous QCT calculations.[10,11,23] We have shown that these product distributions reflect a reaction mechanism where the N atom approaches the interaction region with a large impact parameter. However, the WP and QCT inverted vibrational distributions are different from those observed, which are oscillating and prefer even v' quanta.

In closing, we stress that the WP formalism depends strongly on all the features of the PESs, so that it is a very useful approach for probing potential surfaces. We have shown that the recent S3 PES (Ref. 7) of the $X\ ^2A'$ state behaves correctly nearly everywhere, whereas the $a\ ^4A'$ PES needs some refinements. In comparing WP and observed thermal rate constants, we have found that the S3 barrier height should be probably lowered by $\sim$0.0245 eV. Since this value is equal to 0.56 kcal/mol, this PES has reached a chemical accuracy within 1 kcal/mol. We are currently improving the quartet surface of Ref. 7, calculating more *ab initio* points in the O+N+O product channel, and carrying out an improved analytical fit of this repulsive region of the PES.

ACKNOWLEDGMENTS

One of the authors (C.P.) thanks Dr. S. Gray for a copy of his wave-packet codes and for many useful discussions. C.O. thanks the Spanish Ministry of Education and Culture for a visiting research grant at the University of Siena. This work has been supported by MIUR (Programmi di Ricerca Scientifica di Rilevante Interesse Nazionale), by the Universita' di Siena (Progetti di Ricerca), by the IPCF-CNR of Pisa, by the Dirección General de Enseñanza Superior (Programa Sectorial de Promoción General del Conocimiento) of the Spanish Ministry of Education and Culture (DGES Project Ref. PB 98-1209-C02-01), and by the European Union (INTAS Project Ref. 99-00701).

[1] D. L. Baulch, C. J. Cobos, R. A. Cox, G. Hayman, T. Just, J. A. Kerr, T. Murrells, M. J. Pilling, J. Troe, R. W. Walker, and J. Warnatz, J. Phys. Chem. Ref. Data **23**, 847 (1994).
[2] I. C. Winkler, R. A. Stachnik, J. I. Steinfeld, S. J. Lipson, and W. A. M. Blumberg, J. Chem. Phys. **85**, 890 (1986), and references therein.
[3] G. E. Caledonia, R. H. Krech, and D. B. Oakes, J. Geophys. Res. **105**, 12833 (2000).
[4] S. P. Walch and R. L. Jaffe, J. Chem. Phys. **86**, 6946 (1987).
[5] R. Sayós, C. Oliva, and M. González, J. Chem. Phys. **115**, 1287 (2001).
[6] M. González, C. Oliva, and R. Sayós, J. Chem. Phys. (in press).
[7] R. Sayós, C. Oliva, and M. González, J. Chem. Phys. (in press).
[8] P. Defazio, C. Petrongolo, S. K. Gray, and C. Oliva, J. Chem. Phys. **115**, 3208 (2001).
[9] R. Sayós, J. Hijazo, M. Gilibert, and M. González, Chem. Phys. Lett. **284**, 101 (1998).
[10] C. Oliva, Ph.D. thesis, Universitat de Barcelona, Spain, 2001.
[11] J. W. Duff, G. Bien, and D. E. Paulsen, Geophys. Res. Lett. **21**, 2043 (1994).
[12] S. K. Gray and G. G. Balint-Kurti, J. Chem. Phys. **108**, 950 (1998).
[13] A. J. H. Meijer, E. M. Goldfield, S. K. Gray, and G. G. Balint-Kurti, Chem. Phys. Lett. **293**, 270 (1998).
[14] S. K. Gray, C. Petrongolo, K. Drukker, and G. C. Schatz, J. Phys. Chem. A **103**, 9448 (1999).
[15] E. M. Goldfield and A. J. H. Meijer, J. Chem. Phys. **113**, 11055 (2000).

[16] J. M. Bowman, J. Phys. Chem. **95**, 4960 (1991).
[17] H. Koizumi, G. C. Schatz, and M. S. Gordon, J. Chem. Phys. **95**, 6421 (1991).
[18] G. Herzberg, *Molecular Spectra and Molecular Structure* (Krieger, Malabar, 1989), Vol. I, p. 251.
[19] S. K. Gray, G. G. Balint-Kurti, G. C. Schatz, J. J. Lin, X. Liu, S. Harich, and X. Yang, J. Chem. Phys. **113**, 7330 (2000).
[20] D. Bose and G. V. Candler, J. Chem. Phys. **107**, 6136 (1997).
[21] N. Balakrishnan and A. Dalgarno, Chem. Phys. Lett. **302**, 484 (1999).
[22] (a) R. D. Levine and R. B. Bernstein, *Molecular Reaction Dynamics and Chemical Reactivity* (Oxford University Press, New York, 1978), p. 179; (b) p. 274; (c) p. 151.
[23] B. Ramachandran, N. Balakrishnan, and A. Dalgarno, Chem. Phys. Lett. **332**, 562 (2000).